J. Synchrotron Rad. (1998). **5**, 1390–1395

X-ray Imaging and Microspectroscopy of Plants and Fungi

W. Yun,[a]* S. T. Pratt,[b] R. M. Miller,[b] Z. Cai,[a] D. B. Hunter,[c] A. G. Jarstfer,[d] K. M. Kemner,[b] B. Lai,[a] H.-R. Lee,[a] D. G. Legnini,[a] W. Rodrigues[a] and C. I. Smith[b]

[a]Experimental Facilities Division, Argonne National Laboratory, Argonnne, IL 60439-4800, USA, [b]Environmental Research Division, Argonne National Laboratory, Argonne, IL 60439-4843, USA, [c]Savannah River Ecology Laboratory, The University of Georgia, Aiken, SC 29802, USA, and [d]LeTourneau University, PO Box 7001, Longview, TX 75607-7001, USA. E-mail: yun@aps.anl.gov

(*Received 12 February 1998; accepted 19 May 1998*)

X-ray fluorescence microscopy and microspectroscopy with micrometre spatial resolution and unprecedented capabilities for the study of biological and environmental samples are reported. These new capabilities are a result of both the combination of high-brilliance synchrotron radiation and high-performance X-ray microfocusing optics and the intrinsic advantages of X-rays for elemental mapping and chemical-state imaging. In this paper, these capabilities are illustrated by experimental results on hard X-ray phase-contrast imaging, X-ray fluorescence (XRF) imaging and microspectroscopy of mycorrhizal plant roots and fungi in their natural hydrated state. The XRF microprobe is demonstrated by the simultaneous mapping of the elemental distributions of P, S, K, Ca, Mn, Fe, Ni, Cu and Zn with a spatial resolution of approximately 1×3 μm and with an elemental sensitivity of approximately 500 p.p.b. Microspectroscopy with the same spatial resolution is demonstrated by recording near-edge X-ray absorption (XANES) spectra of Mn at a concentration of approximately 3 p.p.m.

Keywords: X-ray microprobes; high spatial resolution; high sensitivity; elemental maps.

1. Introduction

The development of high-brilliance third-generation synchrotron sources such as the Advanced Photon Source (APS), Advanced Light Source (ALS), European Synchrotron Radiation Facility (ESRF) and SPring-8 is expected to result in substantial advances in the state-of-the-art of X-ray spectroscopy, scattering and imaging. In this paper, the utility of such sources for hard X-ray imaging and microspectroscopy of biological and environmental samples is illustrated by new results from the APS. Hard X-ray phase-contrast images, element-specific X-ray fluorescence (XRF) images and X-ray absorption near-edge spectra obtained with focused X-rays (micro-XANES) are all reported. The new data were obtained with a minimal amount of sample preparation and clearly illustrate the potential of the new high-brilliance synchrotrons for considerable improvements in the spatial resolution, data-acquisition time, detection sensitivity and minimization of sample damage associated with these techniques.

The specific microimaging and microspectroscopy studies reported here are focused on the mechanisms for the uptake of metals by mycorrhizal fungi and plants. Approximately 90% of the world's vascular plants, including the majority of all economic crops, belong to families that commonly have symbiotic associations with mycorrhizal fungi (Trappe, 1987; Allen, 1991; Miller, 1987; Marschner, 1995). While such associations are known to increase plant viability under low nutrient conditions, in some instances mycorrhizal fungi can also moderate toxicity effects in plants growing on soils containing elevated concentrations of heavy metals (Bradley *et al.*, 1981, 1982; Galli *et al.*, 1994; Gadd, 1993). Thus, an improved understanding of the plant–fungus relationship, particularly with respect to the uptake mechanisms for metals, is expected to have significant implications in both agriculture and the remediation and restoration of contaminated environments.

X-ray fluorescence microscopy and microspectroscopy can provide information on the spatial distribution, oxidation state, chemical environment and transformations of trace elements (Kirz *et al.*, 1995; Mattigod *et al.*, 1990; Schulze & Bertsch, 1995; Bertsch *et al.*, 1994; Sparks, 1980; Koningsberger & Prins, 1988; Forslind *et al.*, 1991), and offer significant advantages over other techniques. For example, fluorescence signal-to-background ratios are 10 to 10^5 times larger for excitation by X-rays than by charged particles. Thus, although the spatial resolution of electron and proton microprobes can be significantly better than with X-rays, the elemental sensitivity is limited to approximately 100 p.p.m. for electron-induced X-ray

fluorescence and 10 p.p.m. for proton-induced X-ray fluorescence, considerably worse than with X-rays (Forslind *et al.*, 1991). Alternatively, for a given elemental detectability (Sparks, 1980), the radiation dose is 10^{-3} to 10^{-5} times smaller for X-ray excitation. Furthermore, samples for charged-particle microprobes require considerable sample preparation and are difficult to apply to naturally hydrated samples, whereas X-ray microprobes require essentially no sample preparation and can be applied under natural conditions. Finally, chemical-state information is considerably more difficult to obtain with techniques based on charged particles. While soft X-ray (<1 keV) microscopy and microspectroscopy have considerable utility for the study of biological samples (Kirz *et al.*, 1995), the hard X-ray techniques described here provide improved fluorescence yields and access to the *K* edge of the third-row and heavier elements, many of which are important nutrients, micronutrients or environmental contaminants.

Although the intrinsic advantages of X-rays for elemental mapping and chemical-state imaging have long been recognized (Kirz *et al.*, 1995; Mattigod *et al.*, 1990; Schulze & Bertsch, 1995; Bertsch *et al.*, 1994; Sparks, 1980; Koningsberger & Prins, 1988; Forslind *et al.*, 1991), their full potential for imaging could not be realised until bright synchrotron X-ray sources and high-performance X-ray microfocusing optics were developed. Third-generation synchrotron sources such as the APS, where the present experiments were performed, provide an increase in brilliance of approximately three orders of magnitude compared with second-generation synchrotron X-ray sources and approximately nine orders of magnitude compared with conventional X-ray sources. At the same time, advances in microfabrication technologies have resulted in X-ray phase zone plates (Lai *et al.*, 1992) with spatial resolution better than 0.5 μm and focusing efficiency better than 33%. The combination of high-brilliance X-ray sources with high-performance X-ray microfocusing optics results in advances in the state-of-the-art of X-ray microspectroscopy, fluorescence microscopy and phase-contrast imaging. All of the experiments discussed here were performed at the 2-ID-D beamline of the Synchrotron Radiation Instrumentation Collaborative Access Team of the APS (Yun *et al.*, 1996).

2. Experiment and results

Hard X-ray phase-contrast imaging provides a particularly effective method of imaging the sample and locating suitable regions of interest for fluorescence mapping and micro-XANES measurements. The present phase-contrast imaging was performed with a simplified version of a previously employed scheme (Snigirev *et al.*, 1995). This approach is different from the phase-contrast imaging microscope described by Schmahl & Rudolph (1987), and is more similar to the defocus phase-contrast imaging in electron microscopy. Coherent monochromatic X-ray radiation was collimated and passed through the sample and then onto a scintillation screen approximately 1.5 m downstream from the sample. The visible image on the screen was then imaged with a video camera equipped with a 20× or 40× microscope objective. Images were obtained at the video clock rate, and the spatial resolution was approximately 5 μm. Because the absorption contrast of the root-fungus sample at the X-ray energy used (11.9 keV) is very small, the phase change when the X-rays pass through the sample provides the main contrast mechanism for the image. Indeed, phase contrast and absorption contrast can be distinguished by moving the detector close to the sample, where the absorption image dominates. In the present experiments, this absorption image is essentially invisible. Because it is performed with the unfocused X-ray beam in an in-line geometry, phase-contrast imaging provides an image of a selected portion of the sample, and, when the zone plate is moved into place, the focused beam is essentially at the centre of this region.

Fig. 1(*a*) shows an optical micrograph of a *Plantago lanceolata* L. root that has been infected by the arbuscular mycorrhizal fungus *Glomus mosseae* (Nicol. & Gerd.) Gerdemann & Trappe. (The samples were prepared as follows. *Plantago lanceolata* seedlings were transplanted in flint sand and inoculated with approximately 40 spores of *Glomus mosseae*. The plants were watered daily, alternating each day between deionized water and 10% Hoagland's solution. After 45 days the plants were harvested by washing the sand from the roots and fungal hyphae and rinsing with deionized water.) Fig. 1(*b*) shows a phase-contrast image of a similar sample. The raw image in Fig. 1(*b*) has been divided by an image taken with the beam aligned off the sample, which removes features resulting from inhomogeneities in the windows and beamline optics. The thread-like features coming off approximately perpendicular to the root are fungal hyphae. The hyphae can be distinguished from root hairs because they branch and enter the root at multiple points. The spatial resolution of the images in Figs. 1(*a*) and 1(*b*) is comparable. It must be stressed, however, that the sample for the optical image of Fig. 1(*a*) required clarification in KOH to remove cell cytoplasm, neutralization, staining to highlight fungal material, and squash mounting, while that for the phase-contrast image of Fig. 1(*b*) was simply wet mounted between two layers of Kapton tape, a procedure that could even be applied to living plants. Thus, the phase-contrast image shows structures that could be lost or altered in the preparation of the sample for optical imaging. For example, the stele (the central structure) of the wet root in Fig. 1(*b*) would be collapsed in a dried root. In addition, the phase-contrast image required only a few milliseconds of exposure time. Phase-contrast images recorded near the *K* edges of elements of interest are expected to provide elemental selectivity.

The high-performance zone plate used in the present XRF-imaging and microspectroscopy experiments produced a focused beam of 1 μm × 3 μm cross section and

4×10^{10} photons s^{-1} (0.02% bandwidth)$^{-1}$. The zone plate had an effective focal length of 52.5 cm at 11.9 keV and an effective spot size of 1 μm (vertical) by 3 μm (horizontal). The X-ray beam passed through a 20 μm order-sorting aperture and the focus was adjusted to be on the sample. Samples for the XRF images were mounted on a computer-controlled *XYZ* stage at 20° or 45° to the incident X-ray beam. Thus, in the latter case, the 3 μm-wide horizontal beam intercepted approximately 4.2 μm in the horizontal dimension of the sample, while the 1 μm vertical dimension of the beam was preserved. X-ray fluorescence from the sample was collected at 90° to the incident beam by using an energy-dispersive single-element solid-state detector.

Fig. 2 shows a series of images of a wet root-fungus sample for the micronutrients Mn, Fe, Cu and Zn. Similar images were recorded simultaneously for P, K, S, Ca and Ni. The map of an individual element was obtained by scanning the sample in 5 mm steps through the focused monochromatic X-ray beam (11.9 keV) and integrating the selected *Kα* fluorescence for 3 s per point. The total data-collection time for a 61 × 61 pixel array (300 × 300 μm) was approximately 4 h, and the elemental sensitivity was approximately 500 p.p.b. The absolute concentrations were determined by calibrating the detector with standard films from the National Institute of Standards and Technology, but have not been corrected for effects due to attenuation of the emitted X-rays by the sample; they are expected to be accurate to within a factor of two. The concentrations in the figure are given in μg cm^{-2} and the thickness of the sample must be taken into account to estimate the sensitivity of the technique. For thick samples, such as those in Fig. 2, the spatial resolution of both electron- and proton-based microprobes for thick samples would be poorer because the activation due to scattering of the charged particle beams in the sample is much larger (Sparks, 1980). As a result, a meaningful comparison of the sensitivities in terms of μg cm^{-2} is difficult to make.

The distributions of the four elements in Fig. 2 show very different behaviour. Interestingly, there is little evidence for Mn in the fungal hyphae, which may be related to the observation that mycorrhizal plants typically have much lower Mn concentrations than non-mycorrhizal plants (Kothari *et al.*, 1991). The Fe tends to be most concentrated on the edge of the root, perhaps reflecting the precipitation of Fe in this location. Both Cu and Zn show up most strongly in the fungal hyphae and in the centre of the root, most likely in the inner cortex where the proliferation of the fungus is greatest (see Fig. 1*a*). This suggests the use of

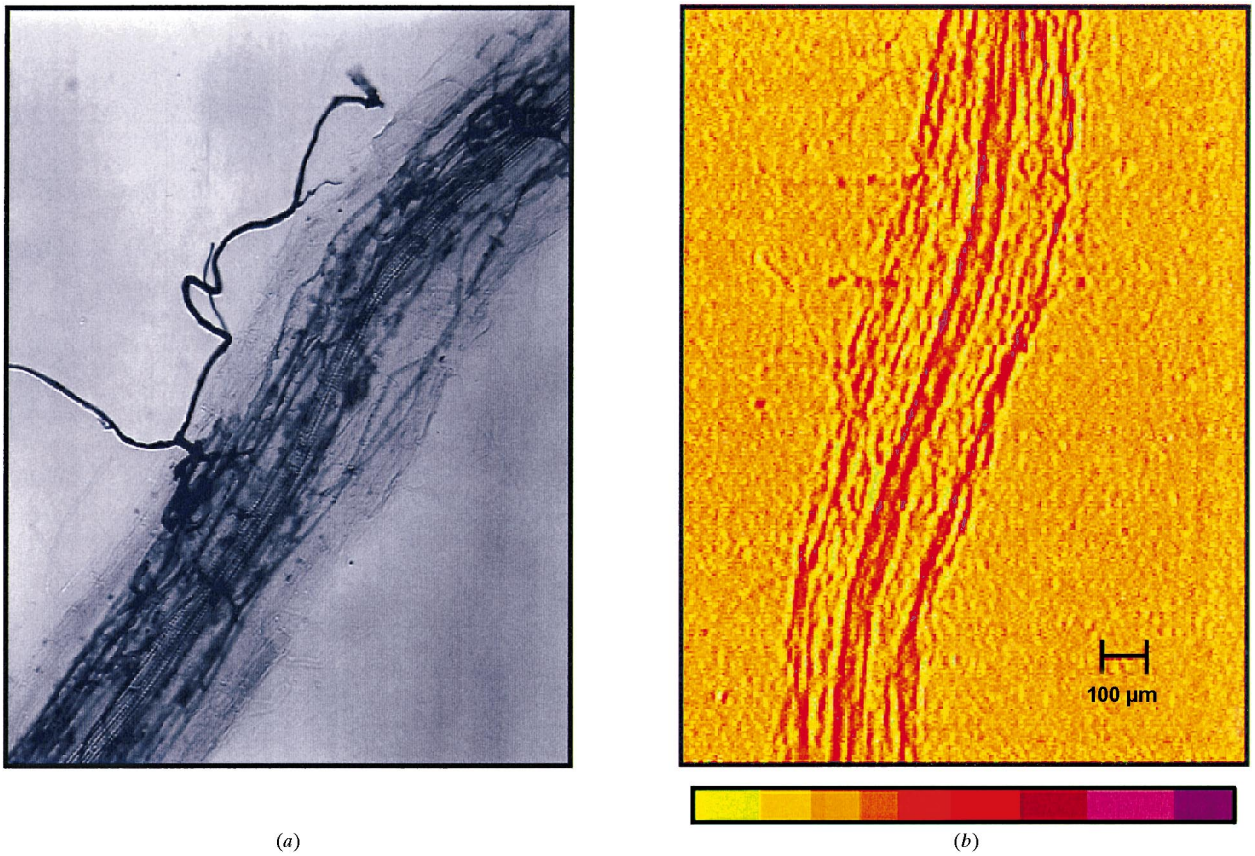

Figure 1
(*a*) An optical micrograph of a clarified and stained *P. lanceolata* root infected by the mycorrhizal fungus *G. mosseae.* (*b*) A hard X-ray phase-contrast image of an unclarified unstained wet *P. lanceolata* root infected by the mycorrhizal fungus *G. mosseae.* The scale bars in (*a*) and (*b*) are of essentially the same size.

Cu and Zn as surrogate measures of mycorrhizal fungi in roots and additional work is underway to confirm this correlation.

An important advantage of using monochromatic radiation in the present experiments is that any scattered radiation can be filtered out because it comes at a single energy in the energy-dispersed fluorescence spectrum (Sparks, 1980). This provides a much lower background than is achievable using white light, which in the past has generally been used to increase signal intensity (Schulze & Bertsch, 1995; Bertsch *et al.*, 1994). The problems associated with white light are exacerbated with wet samples. In addition, although XRF images have been recorded at second-generation sources with white light and 5 μm- to 10 μm-diameter spots, microspectroscopy studies with monochromatic light have typically been performed with 100 μm- to 300 μm-diameter spots (Schulze & Bertsch, 1995; Bertsch *et al.*, 1994; Schulze, McCay-Buis *et al.*, 1995; Schulze, Sutton & Bajt, 1995), and in most cases the sample has been dried.

The determination of both the spatial distribution and the chemical state of selected elements is important for

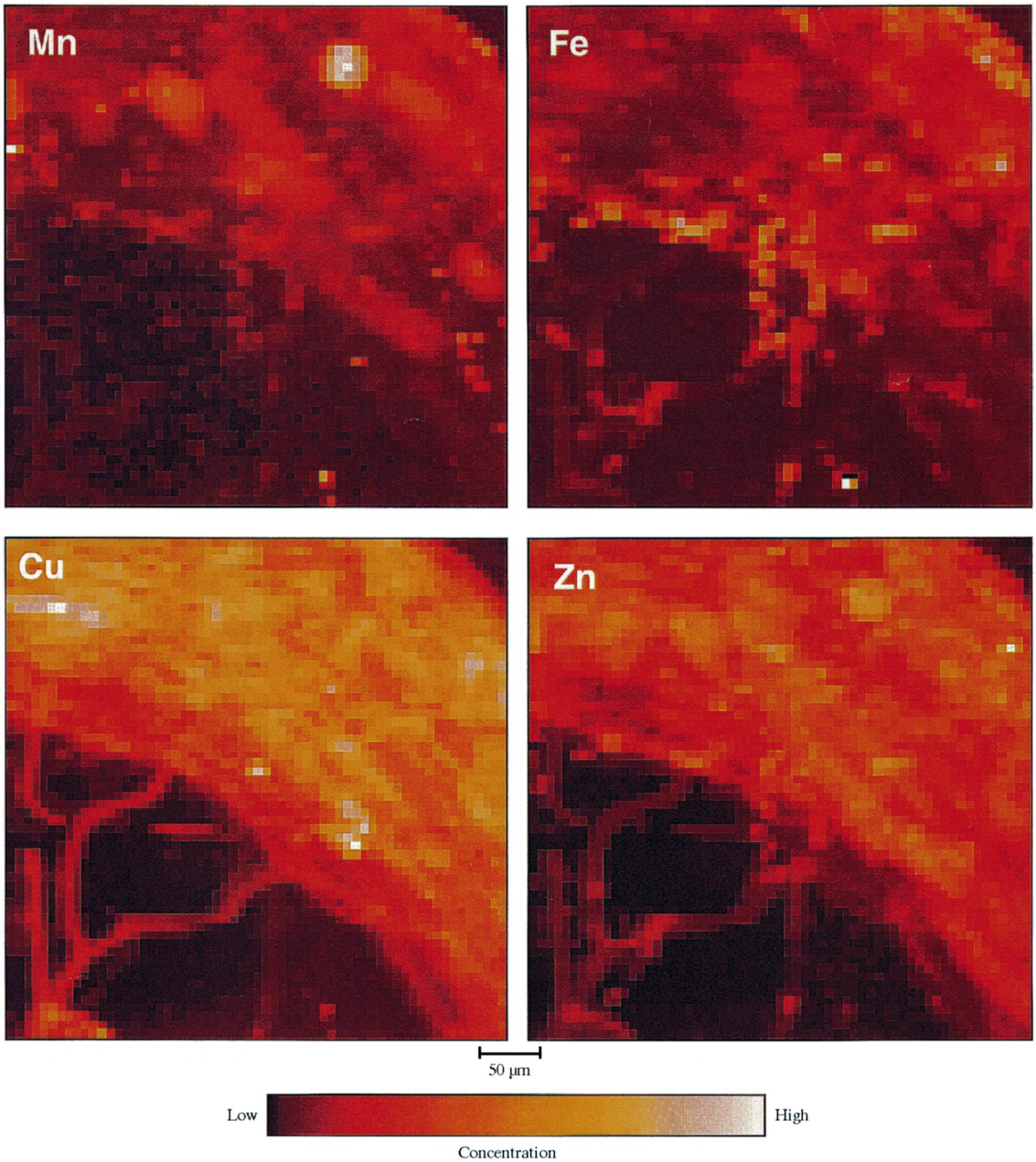

Figure 2
Selected element-specific XRF images of a hydrated *P. lanceolata* root infected by the mycorrhizal fungus *G. mosseae*. The concentration ranges for the individual images are 0.03 to 0.87 μg cm^{-2} for Mn, 0.11 to 27.9 μg cm^{-2} for Fe, 0.03 to 1.55 μg cm^{-2} for Cu, and 0.04 to 4.98 μg cm^{-2} for Zn. The concentrations have not been corrected for small changes in the X-ray beam intensity or for the attenuation of the X-ray fluorescence by the sample, and may only be accurate to within a factor of two.

many problems in biology and environmental science. For such studies it is essential that the sample be in its natural hydration state because drying could modify the chemical form of the element of interest. To demonstrate the enhanced capabilities provided by a high-brilliance X-ray source and the use of high-performance zone plates, we recorded micro-XANES spectra at the Mn *K* edge with a 1×3 μm spot size at selected positions within the hydrated sample shown in Fig. 1(*b*). Mn is an essential micronutrient in both plants and fungi, and in natural systems it usually exists in the +2 or +4 oxidation state; the +3 oxidation state is also possible but is generally unstable.

The XANES spectra were recorded by aligning the focused X-ray beam to several different spatial features in the root and fungal hyphae and scanning the X-ray energy through the absorption edge while monitoring the Mn $K\alpha$ fluorescence. The spatial resolution and sensitivity of the present experiments allow the study of a single fungal hypha. Fig. 3 shows an Mn micro-XANES spectrum with the beam aligned to the stele in the centre of the root. Each point in the spectrum was averaged for 10 s of detector live time, and the full spectrum was recorded in approximately 45 min. The spectrum has been normalized by dividing the fluorescence signal by the intensity of the transmitted light, and energy calibrated by using an elemental Mn standard. The focal length of the zone plate depends on wavelength and, in principle, the distance of the zone plate to the sample should be scanned as the X-ray energy is scanned. Because the XANES spectra cover a limited energy range, however, no attempt was made to scan the zone-plate distance in the present experiments. It is estimated that the effective spot size varies from approximately 1 to 2 μm in the vertical direction and from 3 to 3.6 μm in the horizontal direction. In this sample, the Mn XANES spectrum was found to be independent of position, and the shapes of all of the spectra were essentially indistinguishable from the one in Fig. 3. Comparison of our results with detailed XANES studies of a wide variety of samples and standards (Schulze, McCay-Buis *et al.*, 1995; Schulze, Sutton & Bajt, 1995; Manceau *et al.*, 1992*a*,*b*) indicated that at least 90% of the Mn sampled by the X-ray beam at each of the locations is Mn^{+2}, the soluble and most useful form to plants and fungi. The lack of variation in the Mn oxidation state in the present sample limits the ability to demonstrate the spatial resolution of the microspectroscopy unequivocally; however, the experiments clearly indicate that we now have the ability to record high-quality XANES spectra with 1 to 2×3 μm spatial resolution and at concentrations of approximately 3 p.p.m. In principle, similar measurements for other third-row and heavier elements should be straightforward.

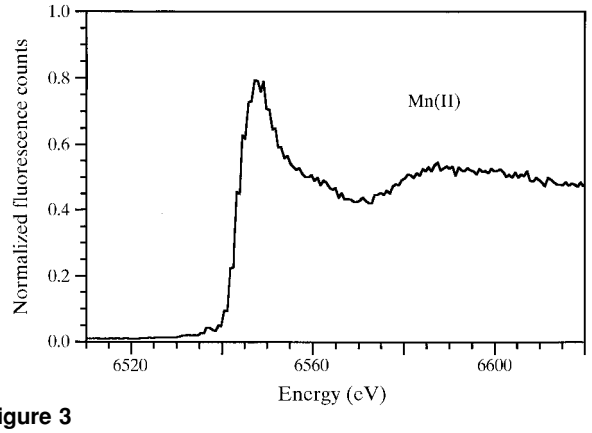

Figure 3
The micro-XANES spectrum at the Mn *K* edge obtained with a 1×3 μm focal spot aligned to the stele in the central portion of the root shown in Fig. 1(*b*). Comparison of the spectrum with known standards indicates that at least 90% of the Mn is in the +2 oxidation state.

The commissioning of new imaging beamlines at the APS and other third-generation synchrotron sources is expected to result in the application of the improved techniques described here to a broad range of issues in the biological and environmental sciences.

This work was supported by the US Department of Energy, Office of Energy Research, Office of Basic Energy Science and Office of Health and Environmental Research, under contract W-31-109-Eng-38, and by financial assistance award No. DE-FC09-965R18546 from the US Department of Energy to the University of Georgia Research Foundation.

References

Allen, M. F. (1991). *The Ecology of Mycorrhizae.* Cambridge University Press.
Bertsch, P. M., Hunter, D. B., Sutton, S. R., Bajt, S. & Rivers, M. L. (1994). *Environ. Sci. Technol.* **28**, 980–984.
Bradley, R., Burt, A. J. & Read, D. J. (1981). *Nature (London)*, **292**, 335–337.
Bradley, R., Burt, A. J. & Read, D. J. (1982). *New Phytol.* **91**, 197–209.
Forslind, B., Malmquist, K. G. & Pallon, J. (1991). *Scanning Microsc.* **5**, 877–884.
Gadd, G. M. (1993). *New Phytol.* **124**, 25–60.
Galli, U., Schüepp, H. & Brunold, C. (1994). *Physiol. Plant.* **92**, 364–368.
Kirz, J., Jacobsen, C. & Howells, M. (1995). *Q. Rev. Biophys.* **28**, 33–130.
Koningsberger, D. C. & Prins, R. (1988). *X-ray Absorption: Principles, Applications, Techniques of EXAFS, SEXAFS and XANES.* New York: Wiley.
Kothari, S. K., Marschner, H. & Römheld, V. (1991). *New Phytol.* **117**, 649–655.
Lai, B., Yun, W., Legnini, D., Xiao, Y., Chrzas, J., Viccaro, P. J., White, V., Bajikar, S., Denton, D. & Cerrina, F. (1992). *Appl. Phys. Lett.* **61**, 1877–1879.
Manceau, A., Gorshkov, A. I. & Drits, V. A. (1992*a*). *Am. Mineral.* **77**, 1133–1143.
Manceau, A., Gorshkov, A. I. & Drits, V. A. (1992*b*). *Am. Mineral.* **77**, 1144–1157.
Marschner, H. (1995). *Mineral Nutrition of Higher Plants*, 2nd ed. New York: Academic Press.
Mattigod, S. V., Rivers, M. L. & Sutton, S. R. (1990). Report ANL/APS/TM-7, pp. 101–124. Argonne National Laboratory, Argonne, IL, USA.

Miller, R. M. (1987). *The Ecophysiology of VA Mycorrhizal Plants*, edited by G. R. Safir, pp. 135–170. Boca Raton: CRC Press.

Schmahl, G. & Rudolph, D. (1987). *X-ray Microscopy*, edited by P. C. Cheng & G. J. Jan, pp. 231–238. Berlin: Springer-Verlag.

Schulze, D. G. & Bertsch, P. M. (1995). *Adv. Agron.* **55**, 1–66.

Schulze, D. G., McCay-Buis, T., Sutton, S. R. & Huber, D. M. (1995). *Phytopathology*, **85**, 990–994.

Schulze, D. G., Sutton, S. R. & Bajt, S. (1995). *Soil Sci. Soc. Am. J.* **59**, 1540–1548.

Snigirev, A., Snigireva, I., Kohn, V., Kushnetsov, S. & Schelokov, I. (1995). *Rev. Sci. Instrum.* **66**, 5486–5492.

Sparks, C. J. Jr (1980). *Synchrotron Radiation Research*, edited by H. Winick & S. Doniach, pp. 459–512. New York: Plenum Press.

Trappe, J. M. (1987). *The Ecophysiology of VA Mycorrhizal Plants*, edited by G. R. Safir, pp. 2–25. Boca Raton: CRC Press.

Yun, W., Lai, B., Shu, D., Khounsary, A., Cai, Z., Barraza, J. & Legnini, D. (1996). *Rev. Sci. Instrum.* **67**(9). CD-ROM.